COMPARISONS BETWEEN EXPERIMENTAL MEASUREMENTS AND RANS-Based SIMULATIONS ON THE AERODYNAMICS OF A HORSESHOE VORTEX CONFIGURATION

Demos P. Georgiou[a] *- Kypros F. Milidonis*[b] *- Anestis I. Geniketzidis*[c]

[a, b, c] University Of Patras, Department of Mechanical Engineering and Aeronautics,
Thermal Engines Laboratory, Rion – Patras 26500, Greece

[b]Corresponding author
milidon@mech.upatras.gr

[a]dpgeorg@mech.upatras.gr
[c] gmrf1@yahoo.gr

ABSTRACT

Rans – based simulations are often used in order to simulate the highly three dimensional nature of the flow close to the junction area of cascades or other horseshoe vortex configurations. Despite the enormous development of CFD methods and turbulence models of the past decade, the accurate prediction of secondary flows and heat transfer phenomena in blade to blade passages is still considerably a very challenging task. The present study employs the *k-ω* Shear Stress Transport (SST) model in order to simulate the secondary flow structures past a symmetric body attached on an endwall and compares the predictions to detailed experimental data obtained on an identical geometry. The experimental data provided an evaluation of how accurately the $k-\omega\ SST$ model can predict the behavior and spatial position of the horseshoe vortex core as it wraps around the leading edge of the bluff body.

Nomenclature

X_{up}	Distance upstream the leading edge of the Bluff Body
D	Bluff Body leading edge diameter (**mm**)
$\boldsymbol{r}^*$	Non dimensional radius (= $\mathbf{r/R_{LE}}$)
R_{LE}	Bluff Body leading edge radius (**mm**)
θ	Angular plane position (°)
u	Local velocity ($\mathbf{m/s}$)
V	Velocity Magnitude ($\mathbf{m/s}$)
$\boldsymbol{U}_\infty$	Freestream air velocity ($\mathbf{m/s}$)
CPs	Coefficient of Static Pressure ($= (\mathbf{P}-\mathbf{P}_\infty)/(\mathbf{0.5}.\boldsymbol{\rho}_{\mathbf{air}}.\mathbf{U}_\infty^{\mathbf{2}})$)
$\boldsymbol{P}_\infty$	Freestream pressure remote from any disturbance (**Pa**)
P	Local Static Pressure (**Pa**)
Ω	Vorticity Magnitude (Max Normalized)
ρ	Freestream fluid density (kg/m^3)

1. INTRODUCTION

It has been perceived and understood by now, that the symmetry plane area close to the generic junction of a symmetric bluff body mounded on an endwall, is strongly dominated by the presence of largely three dimensional secondary flows (e.g. York et al. (1984)), often termed as the

"horseshoe vortex system" due to its particular shape. The latter is formed due to the reorganization of the boundary layer vorticity, impinging on the bluff body which generates an adverse pressure gradient on its leading edge symmetry line (Simpson (2001)). The latest models for the aforementioned flow structures were proposed by Langston (1980), Sharma and Buttler (1987) Goldstein and Spokes (1988) and Wang et al. (1997) by means of a vortex model in a cascade arrangement.

Numerical predictions of turbine blade endwall flows are usually investigated via means of turbine cascades in an attempt to simulated and reproduce within acceptable limits of accuracy the secondary flow field and the associated endwall heat transfer obtained from large scale experimental models (Langston et al. (1977), Giel et al. (1996), Kang et al. (1999)). A study by Smirnov (2009) reveals the numerical simulation progress of highly three dimensional turbulent flows and the associated heat transfer made in the past decade and makes a thorough review of the associated studies. The latter constituted an extension to a review made earlier by Langston (2001) who stated the achievements and shortcomings of secondary flows predicted by CFD analyses until that time. Both studies highlight the fact that despite the achievements made, the accurate reproduction of junction flows still remains a challenging task.

On the other hand, generic junction configurations of endwall mounded symmetric bodies immersed in a freestream fluid (e.g. Devenport and Simpson (1990), Hada (2008)) are often employed in order to study the characteristics of the junction flows and their effect on the endwall heat transfer. The recently studied symmetric airfoil junction configuration by Praisner and Smith (2006a, 2006b) is one of the most employed geometries for numerical predictions, because of the experimental data available to compare. RANS-based simulations on the latter geometry were performed by Levchenya et al. (2010) utilizing the low-Re Wilcox (1993) turbulence model as well as the improved Shear Stress Transport (SST) model by Menter (1994) in order to investigate their accuracy on the predicted junction secondary flows and endwall heat transfer. The results showed the advantage of the SST model to qualitatively give correct results when compared to the standard *k-ω* model. Furthermore, in a study performed by Apsley and Leschiziner (2001), the SST model by Menter was found to give the best results in terms of aerodynamic effects and endwall heat transfer when compared to several other RANS-based models. The latter simulations corresponded to the configuration used in the experimental wing-body junction of Devenport and Simpson (1990). In addition in a study performed by Batten et al. (1999), the authors employed various generic junction configurations and performed numerical simulations using RANS turbulence models. In the latter it was shown that obtaining the multiple horseshoe vortices pattern is rather sensitive to both, the turbulence model as well as the grid resolution used. Simulations of wing-body junctions similar to the one tested for the current study are summarized in the study made by Fu et al. (2007), in which a simulation of a wing-body junction flow is also presented. In the latter, hybrid RANS/LES methods are employed for the simulation in order to accurately predict the turbulent kinetic energy and shear stress to obtain a better match to experimental data on the same configuration. It should be noted here that the present study is focused only at two-equation linear eddy viscosity models while the high order Reynolds-stress models (which are also RANS-models) are not considered.

Earlier RANS-based studies made by several teams have shown the inability of the respective turbulence model used, to predict the multiple horseshoe vortex system configuration due to the relatively coarse computational grid employed for the calculations (e.g. Yoo and Yun (1994):standard $k-epsilon$, Lee and Yoo (1997):$RNG\ k-epsilon$, Ivanov et al. (2002):standard k-epsilon and Spalard-Allmaras). On the other hand, a grid sensitivity study made by Levchenya and Smirnov (2007) employing several turbulence models (Wilcox (1993) $k-\omega$ model, Menter (1994) SST model and the non-linear eddy viscosity model v^2-f by Durbin (1991)) for a transonic turbine blade cascade, has concluded that rather fine computational grids are needed to

accurately predict the three dimensional structure of the horseshoe vortex system. However, in the latter it is stated that the Menter SST model is considerably more sensitive to grid refinement but accurately predicts the flow topology and the associated heat transfer. The Menter (1994) SST model was also employed in a study by Levchenya et al. (2009) in which it was found to predict reasonably accurate the complex horseshoe vortex flow patterns. In a study made by Sveningsson (2003) regarding secondary flows originating from the vane-endwall junction, it is concluded that the Durbin $v^2 - f$ followed by $RNG\ k - epsilon$ model was found to give the best agreement when compared to experiments, while the Realizable $k - epsilon$ model was found as the weaker model to predict the associated secondary flow. The $RNG\ k - epsilon$ model along with a fine computational grid was also used in simulations regarding vane filleting situations (e.g. Zess and Thole (2002), Hermanson and Thole (2000)) in which the results showed close resemblance to the experimental data.

Due to its familiarity on reproducing and predicting the complex junction flows, for the present study the $k - \omega\ SST$ model is employed in order to simulate the secondary flow structures past a horseshoe vortex configuration. The results are compared against detailed experimental data obtained on an identical geometry. The horseshoe vortex configuration consists of a symmetric streamlined bluff body having a rounded leading edge and attached on an endwall. The simulations were performed by employing the commercial package Ansys Fluent 14.5, while for the experimental data collection, a miniature 5-Hole Pitot probe was employed which was traversed in a fine grid of measurement points using a computed guided two axis traverse mechanism. The comparison between the experimental data and computational predictions provide an insight of how accurately the $k - \omega\ SST$ model can predict the behavior and spatial position of the horseshoe vortex core as it wraps around the leading edge of the bluff body.

2. THE EXPERIMENTAL FACILITY AND INLET FLOW CONDITIONS

The tests were conducted in an open loop, subsonic low speed wind tunnel whose straight duct was $2m$ long, with a constant rectangular cross sectional area of $0.30\ x\ 0.20\ m^2$. The duct was attached to the wind tunnel's exit nozzle. The maximum speed at the exit of this nozzle was about $16\ m/sec$, provided by a centrifugal blower as it is illustrated in Figure 1. The exit nozzle was preceded by a $1.5m$ long settling chamber integrating an array of 8 damping screens and a honeycomb grid at the end. At the exit plane of the nozzle, the flow was measured with a hot wire anemometer and was found to exhibit a maximum turbulence intensity of less than 0.25% and a mean velocity non–uniformity of less than 0.5% against the span-wise average value. A long $2.75m$ diffuser with an 1:1.5 aspect ratio was employed for connecting the centrifugal blower to the settling chamber. The rotational speed of the motor driving the air supplying blower was regulated electronically via frequency inverter.

The second half of the $2m$ long straight test section (Figure 1: instrumented test section) carries the bluff body and the two axis traverse mechanism. The airfoil – like bluff body, having a leading edge diameter of $60mm$ and a streamlined fairing of $210mm$ (Figure 2a), is constrained between the two endwalls of the $2m$ long test section, while the back side of the bluff body coincides to that of exit plane of the test section as illustrated in Figure 3. For the aerodynamic measurements a forward facing $60°$ cone 5-hole miniature Pitot probe having a tip diameter of $0.9mm$ was employed (Georgiou and Milidonis (2014)). The probe was attached on a two dimensional traverse mechanism, driven by stepper motors and controlled by the commercial code LabVIEW. In the latter motion control code, a YZ-plane inspection subroutine was embedded, which enabled the scanning and pressure data acquisition (obtained by the 5-hole probe) at selected measurement planes along the junction corner.

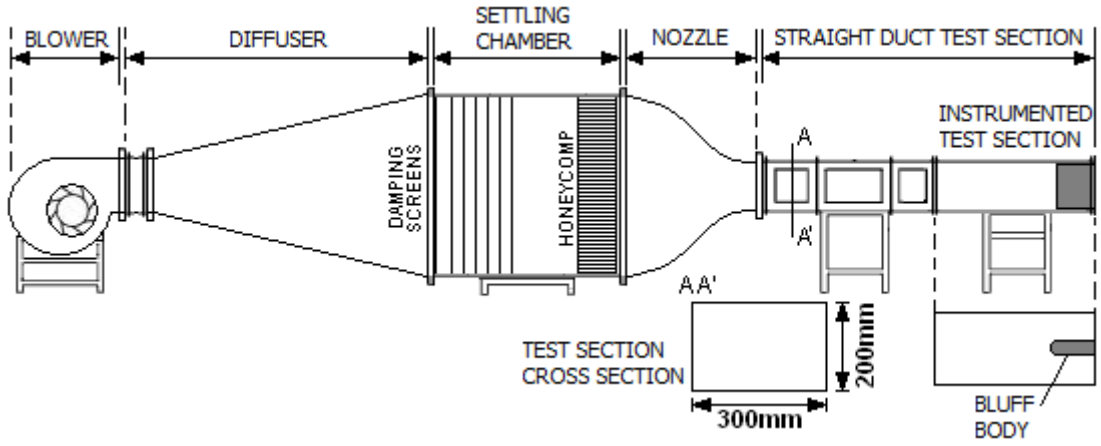

Figure 1: The subsonic, low speed wind tunnel.

In total, 8 planar surfaces were measured downstream the leading edge, while two additional planes were measured at the $\theta = 60°$ and $\theta = 75°$ planes inclined away from the symmetry plane ($\theta = 0°$). The first planar surface is located at $X_{up}/D = -0.5$ downstream the leading edge, while the corresponding location for the last planar surface is located at $X_{up}/D = -3.83$ as illustrated in Figure 2b. The rest of the planes are spaced in between the latter two planes, i.e. every $X_{up}/D = -0.475$.

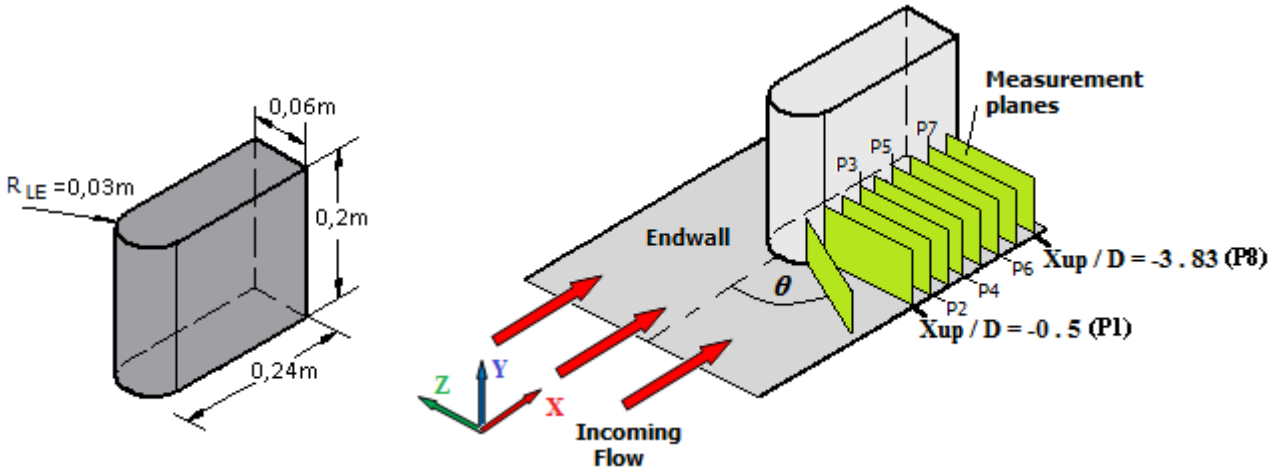

a. b.

Figure 2: a. The bluff body, b. Illustration of the traversed measurement planes

A rectangular grid was chosen having a grid density of $2x2mm$, thus leading to a number of 1180 points for each plane which had a cross sectional area of $118x40mm$. At each point, data were taken at a $2kHz$ frequency over a 2 second interval and the mean values were calculated from the instantaneous values that the probe calibration relationships provided (Georgiou and Milidonis (2014)). The 5-hole Pitot tube signals came from the corresponding high frequency response – highly sensitive differential pressure transducers (Honeywell 164PC01D76) of a $\pm 1.5kPa$ range. The static uncertainty of the transducers was not larger than $\pm 0.05\%$ of the full scale reading. Considering a fully symmetric flow with respect to the leading edge symmetry, the corresponding flowfield was only measured at only one passage (Figure 3a).

3. THE COMPUTATIONAL SETUP

3.1 Problem Definition and Numerical procedure

The geometric characteristics of the under investigation geometry is illustrated in Figure 3 which fully corresponds to the last $1m$ long test section full scale experimental setup. For the purposes of the present numerical study and in order to reduce the computational demands, only half of actual experimental geometry is modeled with respect to the longitudinal symmetry plane (i.e. $YX\ at\ Z = 0m$) and the mid-span plane (i.e. $XZ\ at\ Y = 0.1m$).

3.2 The computational grid

Special care was given on the generation of the computational grid since it is rather sensitive to grid refinement (Levchenya et al. (2007)). After a series of tests regarding the grid independence, the finally adopted grid for calculations nearby consists of more than 18.5 millions cells, from which approximately 9 million of them are located in the passage and leading edge region. In order to obtain the highest quality, a fine hexahedral mesh was used for the rectangular domain upstream of the bluff body. For the latter, a structured C-grid was created around the leading edge and was extended approximately up to 1.5 times the leading edge diameter. Downstream the leading edge the C-grid was again blended to a fine hexahedral mesh. The formulation of the *SST* turbulence model requires that the value of the dimensionless wall distance y+ to be less than 1 near the wall (i.e. endwall) adjacent cells in order to increase the accuracy of the calculated aerodynamic phenomena in the viscosity-affected near wall regions. In order to cope-up to this requirement, the mesh was adjusted in the vertical (Y) direction using a sizing bias. Along the length of the domain and towards the bluff body, the grid was also fixed with also a sizing bias. This led to a very fine mesh towards the bluff body - endwall junction and a relatively coarser mesh at the less important areas. After all mesh treatments, it was identified that the y+ requirement was satisfied more than enough.

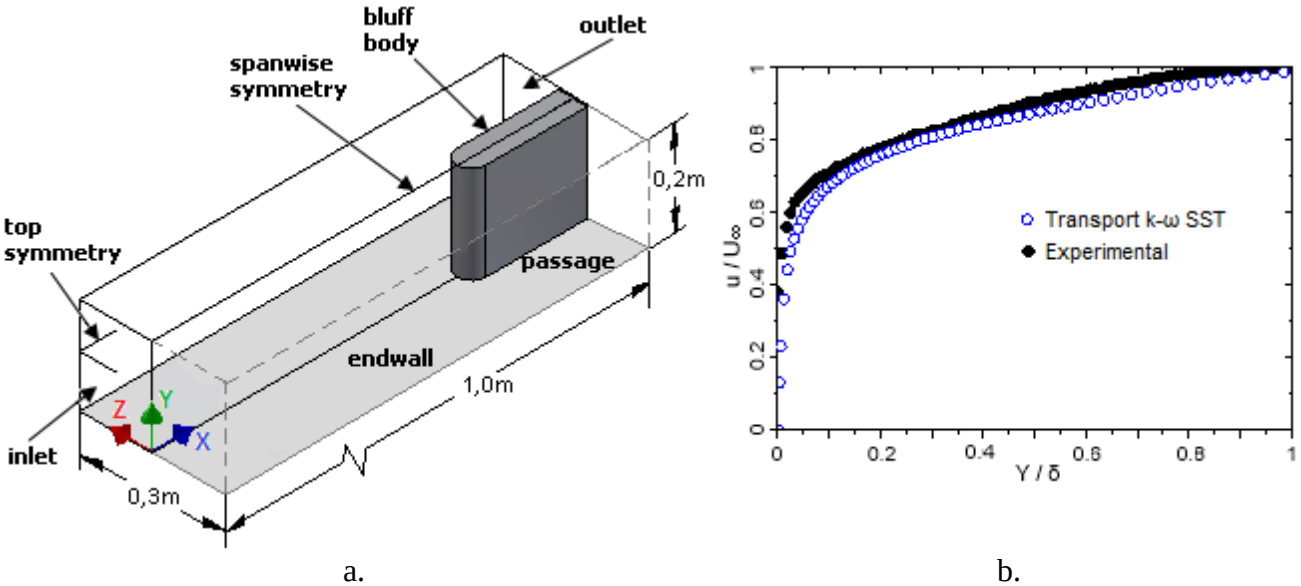

a. b.

Figure 3: a. The physical dimensions and computational domain boundaries of the tested geometry, b. The velocity inlet boundary layer profile at the inlet plane

3.3 The boundary conditions

The inlet section plane, located $0.7m$ upstream of the bluff body's leading edge, it set as a velocity inlet boundary having inflow bulk velocity of $16m/sec$, boundary layer thickness δ of $23mm$ and $0{,}31\%$ freestream turbulence intensity. In order to obtain the inlet velocity characteristics, the full $2m$ long test section was fully simulated beforehand employing the Transition four equation SST model available in Ansys Fluent 14.5 solver. The data obtained from the latter are in good agreement to the experimental data. Figure 3b illustrates a comparison between the simulated and the experimentally measured boundary layer at the corresponding inlet section plane. The outflow for the computational domain is located $0.3m$ downstream the bluff body and was considered as an averaged reference zero pressure. A symmetry condition was applied at the longitudinal spanwise direction which intersects the bluff body in the middle along its longitudinal axis (i.e. $Z = 0m$). The symmetry condition was also applied at the top of the domain since only the half of the test section height was simulated (i.e. bluff body mid-span, $Y = 0.1m$). The walls of the bluff body interacting with the flow are set as no-slip walls. The same stationary, no-slip wall condition is also applied to the endwall. The fluid was considered as incompressible air with density $\rho_{air} = 1.225kg/m^3$ and kinematic viscosity $v = 1.7894x10^{-5}kg/m - s$. The momentum and turbulent characteristics were second order up-winded, while a strict convergence criterion was used since it was set to $1x10^{-5}$ in order for the solution to be considered as converged.

4. RESULTS AND DISCUSSION

Figure 4 provides an isometric view of the predicted computational simulation junction vortex system as it is created and wraps around the bluff body's leading edge and later travels downstream towards the outlet plane. The method used here for the identification of the vortices is the Q-criterion (Hunt et al. (1988)). At the left top corner of Figure 4, the symmetry plane vortex topology is also depicted. The most dominant structure predicted on the symmetry plane is the horseshoe vortex (HV) upstream of which two additional vortex structures are forming (secondary (SV) and tertiary (TV) vortices), due to the collision of the impinging boundary layer with the reverse flow along the endwall. The corner region appears to be dominated by a steady small counter rotating vortex (CV) that fills the gap between the horseshoe vortex and the endwall juncture. In general, the three dimensional flow patterns predicted in the current simulation are in good agreement and are consistent with the four vortex topology model suggested by Arqui and Andreopoulos (1992), Hunt et al. (1978) and Praisner and Smith (2006a, 2006b). The resulting three dimensional secondary flow field in term of streamtraces is shown in Figure 5 as it is experimentally measured at selected planar locations. It should be mentioned here that due to the inherent characteristics of the Pitot probe (i.e. the maximum spatial angle sensitivity is up to $\pm 36°$ for both the pitch and the yaw directions) only planar surfaces at an angle θ greater than 60 degrees could be measured experimentally. Figures 5a and 5b illustrate the relevant flow field at an inclination angle of $\theta = 60°$ (P60) and $\theta = 75°$ (P75) planes respectively, inclined away from the symmetry plane $\theta = 0°$. On the P60 plane the horseshoe vortex core is located at $r^* \cong 1.575$, while later, at the P75 plane the vortex core shifts slightly away from the leading edge. On these two planar locations, the detailed measurements are able to capture the formulation of another vortex upstream of the horseshoe one. Based on its relative position it seems that it corresponds to the tertiary (TV) vortex. On the P1 plane (Figure 5c), which corresponds to the arc end plane of the leading edge ($i.e. \theta = 90°$), the latter vortex is not detected by the measurements due to the fact that the vortex strength is reduced by this location, as it is also predicted by the computational simulation (Figure 4). Nonetheless, the secondary (SV) and tertiary (TV) vortices system is still visible as a detachment of the thin boundary layer outline (which is formed underneath horseshoe vortex) at $r^* \cong 2.00$. In addition, at this angular plane, the horseshoe vortex core is further moved away from the bluff body and it is now located at $r^* \cong 1.702$.

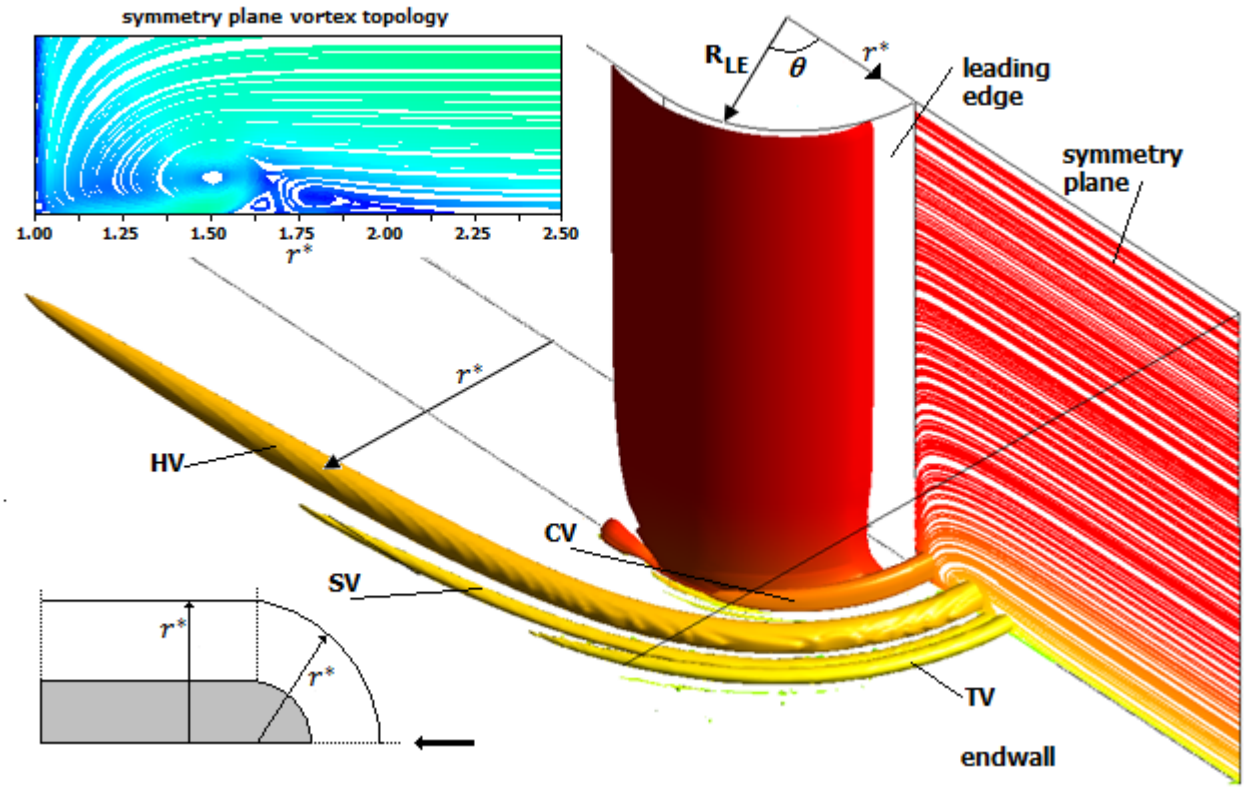

Figure 4: Computational predictions of the junction vortex system (Visualization method: Q-criterion)

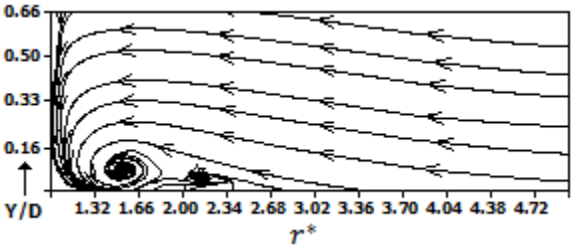

a. ***P60***

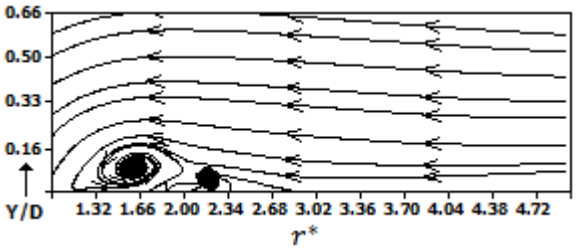

b. ***P75***

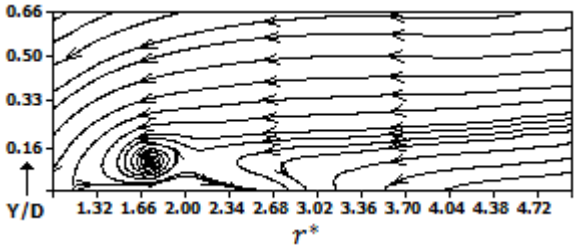

c. ***P1:*** $X_{up}/D = -0.5$

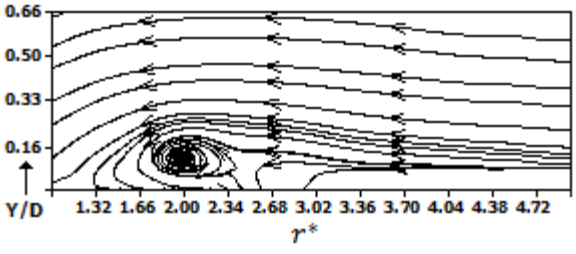

d. ***P4:*** $X_{up}/D = -1.925$

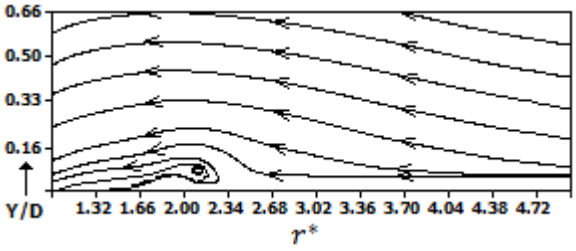

e. ***P7:*** $X_{up}/D = -3.35$

Figure 5: The resulting secondary flow streamtraces as it is experimentally measured at selected planar locations

Almost at the middle of the passage, i.e. at $X_{up}/D = -1.925$ (P4), the horseshoe vortex core is now moved well away from the bluff body at a distance of $r^* \cong 2$, which corresponds nearly to the size of the leading edge radius. Close to the exit plane i.e. at $X_{up}/D = -3.35$ (P7), the strength of the horseshoe vortex is nearly diminished and there exist only weak sighs of its presence.

Figure 6 provides a comparison between the experimentally measured and the computationally predicted trajectory of the horseshoe vortex core as it is deployed around the circumference of the leading edge (i.e. angular planes: $\theta = 0°{\sim}90°$) and moves downstream the passage, towards the exit plane (i.e. planar locations $X_{up}/D = -0.5 \sim -3.825$). It is obvious that there is a very close correlation between the predictions and the measurements, indicating that the simulation can produce qualitatively correct results regarding the position of the horseshoe vortex with respect to the bluff body's solid boundaries. The numerical predictions indicate that the core of the vortex is moving on a concentrically to the leading edge radius of $r^* \cong 1.5$ for an angular position of almost $\theta = 45°$. From thereon, the vortex initiates a drift away from the bluff body leading edge. The distance of the horseshoe vortex core with respect to the bluff body continuously increases towards the exit plane.

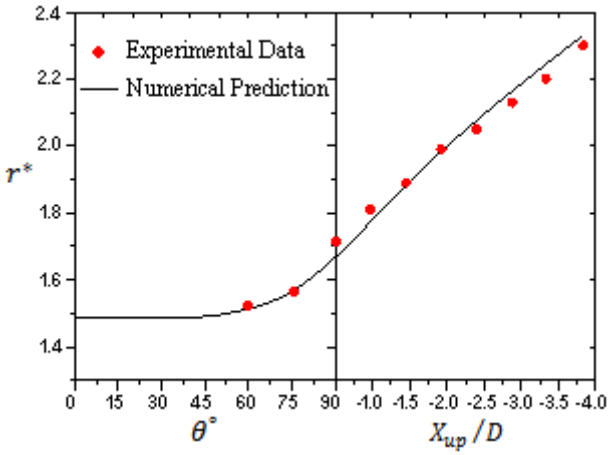

Figure 6: The trajectory of the horseshoe vortex (HV) core: Comparison between experimentally measured and computationally predicted

In order to quantify the accuracy of the numerical predictions, some comparative flow characteristics are investigated between the predictions and measurements for the P75 angular plane.

Figure 7 shows a comparison of the non dimensional velocity magnitude (V/U_∞) contours close to the bluff body - endwall junction and the corresponding secondary flow streamtraces. The velocity magnitude contours in Figures 7a and 7b for the experimental data and numerical predictions respectively, shows similar distributions. As expected, the flow is accelerated close to the vertical wall of the bluff body (i.e. at $r^* \cong 1.00$) as it is moving along the leading edge of the body towards the passage. This acceleration is predicted slightly stronger than it was experimentally measured. Around the horseshoe vortex dominating region (approximately between $r^* \cong 1.32$ to $r^* \cong 1.80$), the iso-velocity lines exhibit disorders due to the rotational movement of the vortex. Again, these disorders appears to be stronger in the predictions than those measured experimentally, probably due to the fine grid employed for the calculations and the weaker grid of the experiments. Taking account Figures 7c and 7d, it is clear that the location and boundaries of the horseshoe vortex are well predicted. Also well predicted is the lift-off point of the streamlines under the vortex at about $r^* \cong 1.66$ which feed the secondary vortex (SV) located between

$r^* \cong 1.66$ and $r^* \cong 2.00$. The experimental measurements do not exhibit clearly the secondary vortex, probably due to its small size which is quite difficult for the Pitot probe to resolve clearly. On the other hand, the core of the larger in size tertiary vortex (TV) is present in the measurements at about $r^* \cong 2.24$ while the corresponding location predicted by the simulation is about $r^* \cong 2.10$.

The distribution of static pressure coefficient (CPs) across a vertical cross section along Y-axis passing through the horseshoe vortex core (i.e. at $r^* \cong 1.585$) is illustrated in Figure 8. The distributions between the predictions and measurements do not exhibit great deviations. The height (Y/D) of the static pressure minima in the vortex core center is predicted well, but the magnitude of the latter is predicted greater than the measurements. The greater discrepancies are observed outside the top boundary of the vortex, approximately after $Y/D = 0.16$.

The corresponding vorticity magnitude (Ω) contours near the bluff body - endwall junction on the P75 angular plane are shown Figures 9a and 9b for the experimental measurements and numerical predictions respectively. The vorticity magnitude shown in the Figures is max normalized based on the corresponding angular plane values of vorticity. Overall, the vorticity patterns are predicted within reasonable accuracy. Both Figures exhibit similar vorticity distributions and the corresponding vorticity values at specific locations (shown in the Figures) exhibit small deviations between the experiment and prediction with some exceptions. The vorticity magnitude predicted for the secondary vortex (i.e. 0.6) is larger than the one measured experimentally (i.e. 0.2) probably due to the weak experimental data obtained in this region.

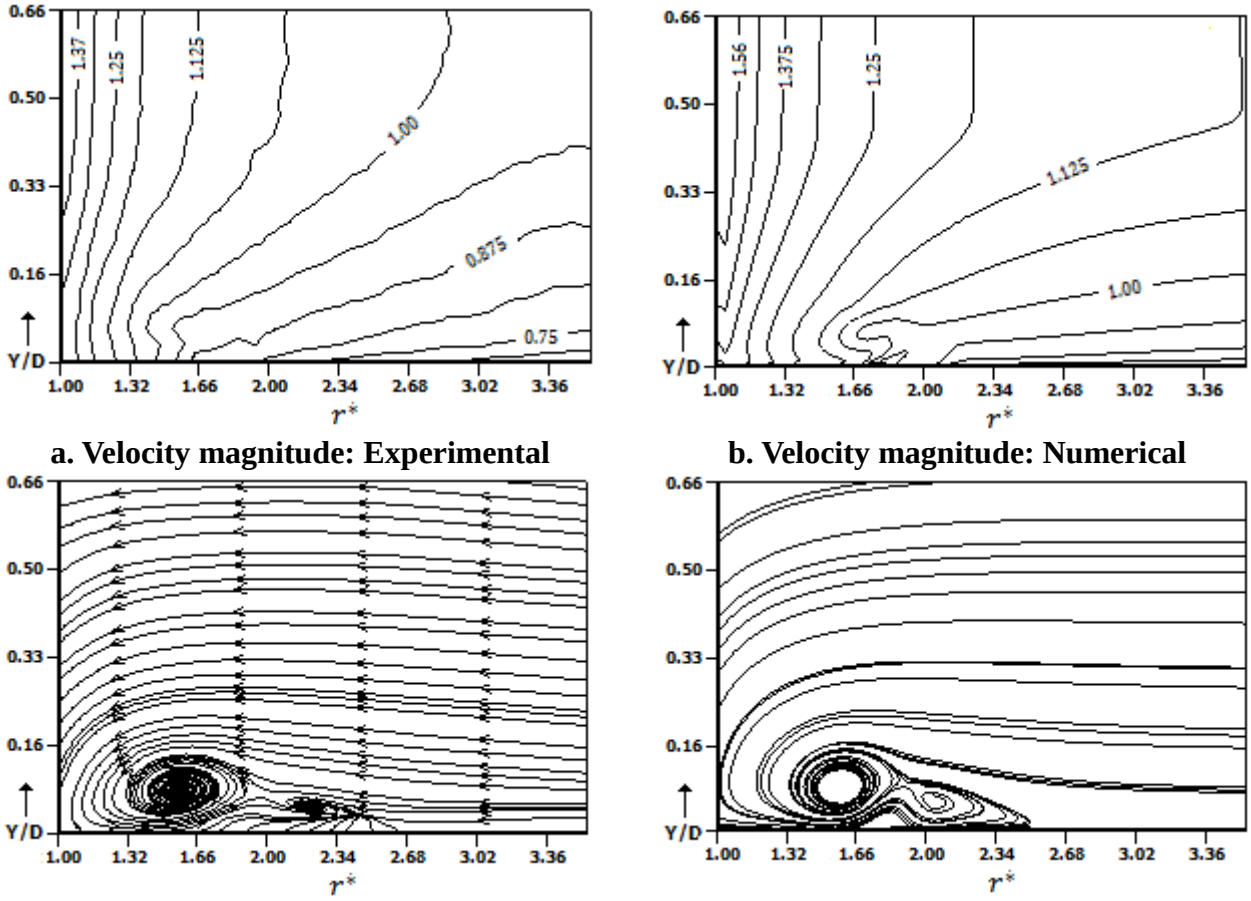

a. Velocity magnitude: Experimental

b. Velocity magnitude: Numerical

c. Secondary flow streamtraces: Experimental

d. Secondary flow streamtraces: Numerical

Figure 7: Contours of velocity magnitude and secondary flow streamtraces close to the bluff body - endwall junction for the P75 angular plane

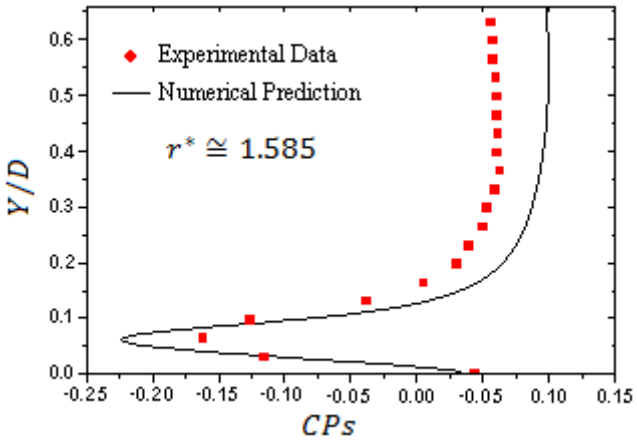

Figure 8: Distribution of static pressure coefficient for a vertical cross section (across Y-axis) passing through the horseshoe vortex core

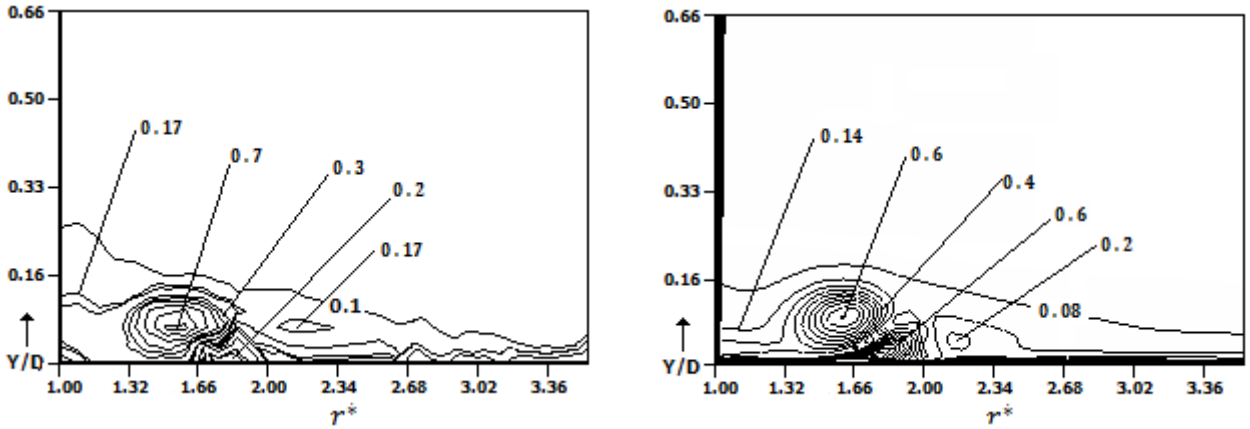

a. Vorticity Contours: Experimental **b. Vorticity Contours: Numerical**

Figure 9: Contours of vorticity magnitude (max-normalized) close to the bluff body - endwall junction for the P75 angular plane

CONCLUSSIONS

A comparison between experimental measurements and RANS-based simulations on the aerodynamics of a horseshoe vortex configuration is presented in the current study. The $k-\omega$ SST model along with a properly formulated computational grid and y+ values of less than 1 near the endwall was found capable to predict the multiple vortex system that develops near the region of a bluff body - enwall junction. The comparative results (experimental and numerical) indicate that the $k-\omega$ SST model can predict fairly accurate and qualitatively the development and spatial position of the horseshoe vortex as it wraps around the leading edge of the bluff body and travels downstream in the passage. In addition, comparing quantitatively the experimental data to the corresponding numerical predictions it is found that the predictions can simulate within reasonable accuracy the relevant flowfield. Of course, it should be stated here that the comparison was made on the basis of the "straight" passage (between the bluff body and the test section walls) which only exhibits the effects of the horseshoe vortex. On the other hand, in cascade arrangements, the three dimensional flow in the passage combines both, the horseshoe vortex and the passage vortex that is

developed due to the curvature of the blades and the strong adverse pressure gradients that dominate the passage area. As a result, the comparative results between experimental data and numerical predictions may not be as accurate as of the current study when applied to an actual cascade arrangement.

REFERENCES

[1] York R.E, Hylton L.D. and Mihelc, M.S., 1984, An experimental Investigation of endwall heat transfer and aerodynamics in a linear cascade, ASME Journal of Engineering for gas turbines and power, Vol. 106, pp. 159-167.

[2] Simpson, R.L., 2001. Junction flows. Annual Review of Fluid Mechanics 33, 415–443.

[3] Langston, L.S., 1980, Crossflows in a Turbine Cascade Passage, Journal of Engineering for Power, Vol. 102, pp. 866-874.

[4] Sharma, O.P. and Butler, T.L., 1987, Predictions of Endwall Losses and Secondary Flows in Axial Flow Turbine Cascades, Journal of Turbomachinery, Vol. 109, pp. 229-236

[5] Goldstein, R.J. and Spores, R.A., 1988, Turbulent Transport on the Endwall in the Region Between Adjacent Turbine Blades, ASME Journal of Heat Transfer, Vol. 110, pp. 862-869

[6] Wang H.P., Olson S.J., Goldstein R.J and Eckert E.R.G., Flow visualization in a linear cascade of high performance turbine blades, Journal of Turbomachinery, 119(1):1-8, 1997

[6] Langston, L. S., Nice, M. L., Hooper, R. M. [1977]. Three-dimensional flow within a turbine cascade passage. ASME J. Eng. Power, Vol. 99, pp. 21-28.

[7] Giel, P.W., Thurman, D.R., Lopez, I., Boyle, R.J., Van Fossen, G.J., Jett, T.A., Camperchioli, W.P., and La, H. [1996]. Three-dimensional flow field measurements in a transonic turbine cascade. ASME Paper 96-GT-113, 14p.

[8] Kang M.B., Kohli A., Thole K.A. [1999]. Heat transfer and flowfield measurements in the leading edge region of a stator vane endwall. ASME J. Turbomach. Vol. 121, pp. 558-567.

[9] Smirnov E.M., Recent developments in numerical simulation of highly three-dimensional turbulent flows and endwall heat transfer in turbine blade cascades, Int. Symp. On Heat Transfer in Gas Turbine Systems, 9-14 August, 2009, Antalya, Turkey.

[10] Langston L.S., Secondary flows in axial turbines – a review, Heat Transfer in Gas Turbine Systems, Annals of the N.Y. Acad. Sci., Vol. 934, pp. 11-26,2001.

[11] Devenport, W. J. and Simpson, R. L. [1990]. Time-dependent and time-averaged turbulence structure near the nose of a wing-body junction. J. Fluid Mech. Vol. 210, pp.23-55.

[12] Hada S., Takeishi, K., Oda, Y., Seijiro Mori, S., and Nuta, Y. [2008] The effect of leading edge diameter on the horse shoe vortex and endwall heat transfer. Proc. ASME Turbo Expo 2008, GT2008-50892

[13] Praisner T.J., and Smith, C.R. [2006a]. The dynamics of the horseshoe vortex and associate

endwall heat transfer – Part I: Temporal behaviorS, ASME J. Turbomach., Vol. 128, pp. 747-754.
[14] Praisner T.J. Smith, C.R. [2006b]. The dynamics of the horseshoe vortex and associate endwall heat transfer – Part II: Time-mean results, ASME J. Turbomach., Vol. 128, pp. 755-762.

[15] Levchenya A.M., Smirnov E.M., Goryachev V.D., RANS-based numerical simulation and visualization of the horseshoe vortex system in the leading edge endwall region of a symmetry body, International Journal of Heat and Fluid Flow 31, 1107-1112, 2010.

[16] Wilcox, D.C., A two-equation turbulence model for wall-bounded and free-shear flows, AIAA Paper 93-2905 (1993).

[17] Menter F.R., Two equation eddy-viscosity turbulence models for engineering applications, AIAA Journal, Vol. 32, 1598-1605 (1994).

[18] Apsley D., and Leschziner, M., Investigation of advanced turbulence models for the flow in a generic wing-body junction. Flow, Turbulence and Combustion, Vol. 67, pp. 25-55, 2001.

[19] Batten P., Craft, T.J., Leschziner, M.A., Loyau, H., Reynolds-stress-transport modeling for compressible aerodynamics applications. AIAA Journal 37 (7), 785–796, 1999.

[20] Fu S. Xiao Z., Chen H., Zhang Y., Huang J., Simulation of wing-body junction flows with hybrid RANS/LES methods, International Journal of Heat and Fluid Flow 28 (2007), 1379-1390, 2007.

[21] Yoo J.Y. and Yun J.W. Comput. Mech., 1994, no. 14, p. 101.

[22] Lee H.G. and Yoo J.Y. Comput. Mech., 1997, no. 20, p. 247.

[23] Ivanov N.G., Levchenya A.M., Ris, V.V., and Smirnov, E.M., The Calculation of Three Dimensional Flow and Heat Transfer in an Experimental Model of Moving Blade Cascade Using One and Two Parameter Models of Turbulence, Proceedings of the 3rd Russian National Conference on Heat Transfer. Vol. II: Forced Convection of Single

[24] Alexander M. Levchenya and Evgueni M. Smirnov, CFD-Analysis of 3D flow structure and endwall heat transfer in a transonic turbine blade cascade: Effects of grid refinement, West-East high speed flow field conference, 19-22, November 2007, Moscow, Russia.

[25] Durbin, P.A., Theor. Comput. Fluid Dyn. 3, 1-13 (1991)

[26] Levchenya A.M., Smirnov E.M., and Goriatchev, V.D. [2009a]. RANS-based numerical simulation and visualization of the horseshoe vortex system in the leading-edge endwall region of a symmetric body. Proc.14th Int. Conf. Fluid Flow Techn., Budapest, September 9-12, 2009, 8 p.

[27] Andreas Sveningsson, Analysis of the Performance of Different $v^2 - f$ T urbulence Models in a Stator Vane Passage Flow, Chalmers University of Technology, Sweden, 2003.

[28] Zess G.A., Thole K.A., Computational design and experimental evaluation of using a leading edge fillet on a gas turbine vane, Journal of Turbomachinery, Vol. 124, 167-175, 2002.

[29] Hermanson, K., and Thole, K. A., Effect of Inlet Profiles on Endwall Secondary Flows, J. Propul. Power, 16, pp 286–296, 2000.

[30] Georgiou D.P, Milidonis K.F., Fabrication and Calibration of a sub-miniature 5-hole probe with embedded pressure sensors for use in extremely confined and complex areas in turbomachinery, Flow Measurement and Instrumentation 39C, pp. 54-63, 2014.

[31] Agui, J.H. and Andreopoulos, J., 1992, Experimental Investigation of a Three-Dimensional Boundary Layer Flow in the Vicinity of an Upright Wall Mounted Cylinder, J. Fluids Eng., Vol. 114, pp. 566-576.

[32] Hunt, J.C.R., Abell, C.J., Peterka, J.A., and Woo, H., 1978, Kinematical Studies of the Flows Around Free or Surface-Mounted Obstacles; Applying Topology to Flow Visualization, J. of Fluid Mech., Vol. 86, Part 1, pp. 179-200.

[33] Hunt J.C.R., Wray A.A., Moin P., 1988. Eddies, stream, and convergence zones in turbulent flows. In: Proceeding of the Summer Program. Center for Turbulence Research. NASA Ames/Stanford University, pp. 193–208.